ARTICLE
PUBLISHED ONLINE: 30 MARCH 2014 | DOI: 10.1038/NCHEMBIO.1496
nature chemical biology

Amphotericin forms an extramembranous and fungicidal sterol sponge

Thomas M Anderson[1,6], Mary C Clay[1,6], Alexander G Cioffi[2], Katrina A Diaz[2], Grant S Hisao[1], Marcus D Tuttle[1], Andrew J Nieuwkoop[1], Gemma Comellas[3], Nashrah Maryum[1], Shu Wang[1,4], Brice E Uno[1], Erin L Wildeman[2], Tamir Gonen[5], Chad M Rienstra[1–3]* & Martin D Burke[1,2,4]*

For over 50 years, amphotericin has remained the powerful but highly toxic last line of defense in treating life-threatening fungal infections in humans with minimal development of microbial resistance. Understanding how this small molecule kills yeast is thus critical for guiding development of derivatives with an improved therapeutic index and other resistance-refractory antimicrobial agents. In the widely accepted ion channel model for its mechanism of cytocidal action, amphotericin forms aggregates inside lipid bilayers that permeabilize and kill cells. In contrast, we report that amphotericin exists primarily in the form of large, extramembranous aggregates that kill yeast by extracting ergosterol from lipid bilayers. These findings reveal that extraction of a polyfunctional lipid underlies the resistance-refractory antimicrobial action of amphotericin and suggests a roadmap for separating its cytocidal and membrane-permeabilizing activities. This new mechanistic understanding is also guiding development of what are to our knowledge the first derivatives of amphotericin that kill yeast but not human cells.

The incidence of life-threatening systemic fungal infections continues to rise in parallel with expanding populations of immunocompromised patients[1]. Substantially exacerbating this problem is the concomitant rise in pathogen resistance to almost all clinically approved antifungal agents. In contrast, since the early 1960s, amphotericin B (AmB) (**Fig. 1a**) has served as the gold standard treatment for systemic fungal infections with minimal development of clinically important microbial resistance[2]. This exceptional track record reveals that resistance-refractory modes of antimicrobial action exist, and the mechanism by which AmB kills yeast is one of them. However, because of the often dose-limiting toxicity of this natural product, mortality rates for systemic fungal infections persist near 50% (ref. 3). Improving the notoriously poor therapeutic index of this drug and the development of other resistance-refractory antimicrobial agents thus represent two critically important objectives that stand to benefit from a clarified molecular description of the biological activities of AmB. Moreover, an advanced understanding of the biophysical interactions of this natural product within living systems would enable the more effective use of its remarkable capacity to perform ion channel–like functions.

For decades, the prevailing theory has been that AmB primarily exists in the form of small ion channel aggregates that are inserted into lipid bilayers and thereby permeabilize and kill yeast cells (**Fig. 1b**)[4–23]. An extensive series of structural and biophysical studies, including those employing planar lipid bilayers[4–10], liposome permeability[9–13,17], Corey-Pauling-Kulton modeling[7–9], UV-visible (UV-vis) spectroscopy[9–11,13,21], CD[10,11,13,21], fluorescence spectroscopy[9,11], Raman spectroscopy[10], differential scanning calorimetry[9,10,21], chemical modifications[11–14,17], atomic force microscopy[21], transmission electron microscopy (TEM)[20], computer modeling[11,15], EPR[10], surface plasmon resonance[22], solution NMR spectroscopy[11] and solid-state NMR (SSNMR)[16–19] spectroscopy have been interpreted through the lens of this ion channel model. Notably, this model suggests that the path to an improved therapeutic index requires selective formation of ion channels in yeast versus human cells[10–20], that the search for other resistance-refractory antimicrobials should focus on membrane-permeabilizing compounds[24] and that the ion channel-forming and cytotoxic activities of AmB cannot be separated.

Recent studies show that the channel-forming capacity of AmB is not required for fungicidal activity, whereas binding ergosterol (Erg) (**Fig. 1a**) is essential[25–27]. However, the structural and biophysical underpinnings of this rare type of small molecule–small molecule interaction and its connection to cell killing remained unclear. Sterols, including Erg in yeast, have many essential roles in eukaryotic cell physiology, including functional regulation of membrane proteins, microdomain formation, endocytosis, vacuole fusion, cell division and cell signaling[28–31]. We thus hypothesized that sequestering Erg and thereby concomitantly precluding its participation in multiple cellular functions may underlie the fungicidal action of AmB.

Guided by this hypothesis, we considered three possible models for the primary structure and function of AmB in the presence of Erg-containing phospholipid membranes (**Fig. 1b–d**): (i) in the classic channel model, AmB primarily exists in the form of small (~1 nm) ion channel aggregates inserted into the membrane, perpendicular to the membrane surface, with Erg molecules interdigitated between AmB molecules (**Fig. 1b**)[7–9,11,12,15–19,22,23]. (ii) In an alternative surface adsorption model, AmB is primarily positioned in the intermediate–head group region, oriented parallel to the plane of the membrane, sequestering Erg to the membrane surface (**Fig. 1c**)[9,22]. (iii) In a new sterol sponge model, AmB primarily exists as large extramembranous aggregates that extract Erg from lipid bilayers (**Fig. 1d**). In the latter two models, we envisioned that membrane-permeabilizing ion channels represent relatively minor contributors to both the structure and cytocidal

[1]Department of Chemistry, University of Illinois at Urbana-Champaign, Urbana, Illinois, USA. [2]Department of Biochemistry, University of Illinois at Urbana-Champaign, Urbana, Illinois, USA. [3]Center for Biophysics and Computational Biology, University of Illinois at Urbana-Champaign, Urbana, Illinois, USA. [4]Howard Hughes Medical Institute, University of Illinois at Urbana-Champaign, Urbana, Illinois, USA. [5]Howard Hughes Medical Institute, Janelia Farm Research Campus, Ashburn, Virginia, USA. [6]These authors contributed equally to this work. *e-mail: rienstra@illinois.edu or burke@scs.illinois.edu

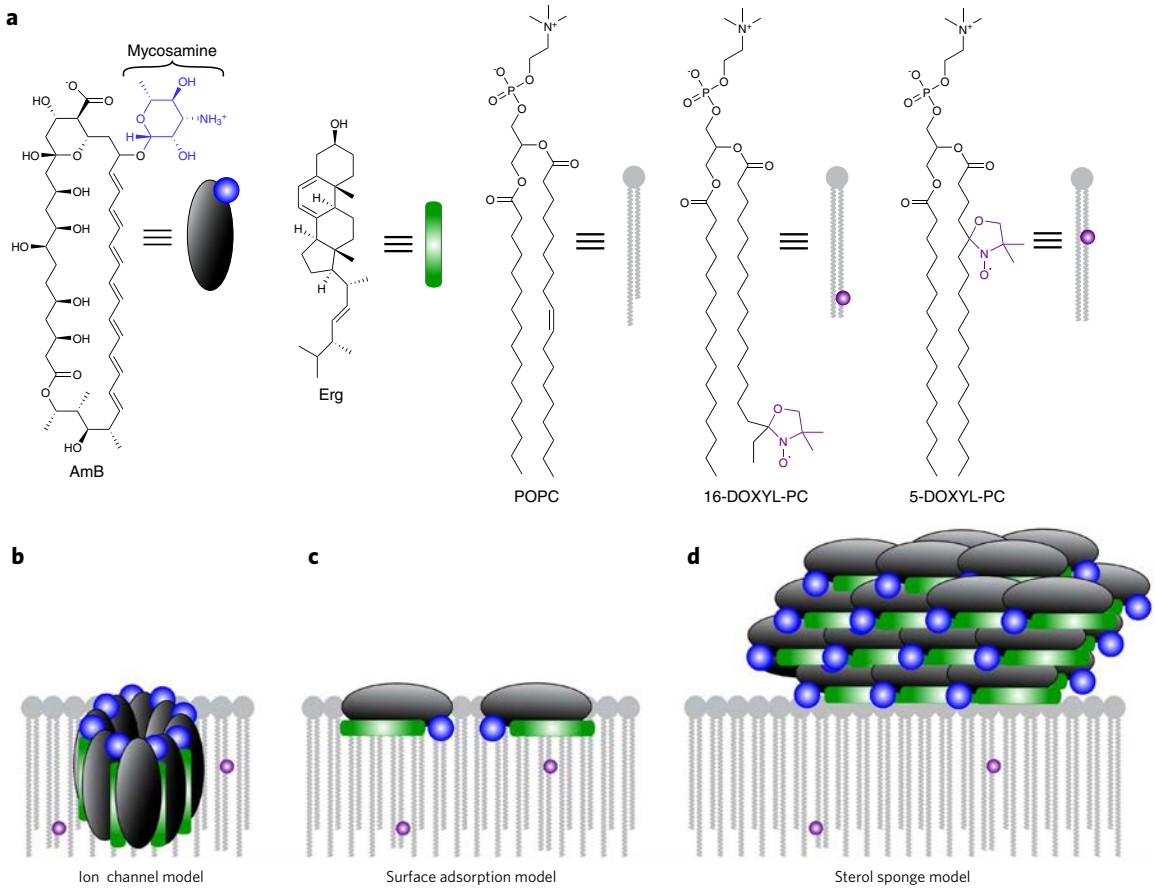

Figure 1 | Models for the structure and function of AmB in the presence of lipid bilayers. (**a**) Structures of AmB, Erg, POPC and paramagnetic probes 5-DOXYL-PC and 16-DOXYL-PC. 5-DOXYL and 16-DOXYL position a paramagnetic functional group at depths of ~12 Å and ~25 Å within the lipid bilayer, respectively. (**b**) The classic ion channel model for the structure and function of AmB. (**c**) Surface adsorption model. (**d**) A new sterol sponge model, in which AmB primarily exists in the form of large extramembranous aggregates that extract Erg from lipid bilayers.

activity of AmB. Here we report an extensive series of SSNMR, TEM and cell-based experiments that all support the new sterol sponge model (**Fig. 1d**).

RESULTS

SSNMR paramagnetic relaxation enhancement experiments

Distinguishing among the aforementioned structural and functional models (**Fig. 1b–d**) required determining the location of AmB relative to lipid bilayers and the corresponding location of Erg in the absence and presence of AmB. Making these determinations turned out to be exceptionally challenging owing to the lack of high-resolution methods for probing small molecule–membrane interactions[9–13,15,17–21]. We thus developed an experiment based on the NMR paramagnetic relaxation enhancement (PRE) of ^{13}C nuclei caused by lipid-appended spin labels[32–34]. ^{13}C nuclei proximal to a stable radical, such as 4,4-dimethyloxazolidine-*N*-oxyl (DOXYL), experience large enhancements of their longitudinal relaxation rates ($R_1 = 1/T_1$). Owing to the high gyromagnetic ratio of the electron spin, the PRE is detectable for distances up to ~20 Å. Harnessing this phenomenon, we designed a magic-angle spinning (MAS) SSNMR PRE experiment based on 16-DOXYL-PC and 5-DOXYL-PC to interrogate proximity to the hydrophobic core and intermediate–head group region, respectively (**Fig. 1a**). Notably, the three models under consideration (**Fig. 1b–d**) predict distinct PRE effects for AmB. The ion channel model predicts large PRE values with both spin labels, the surface adsorption model predicts large PRE values only with 5-DOXYL-PC and the sterol sponge model predicts little or no PRE effects with either spin label.

To execute this experiment with maximized signal-to-noise ratio, we prepared highly enriched uniformly ^{13}C-labeled AmB ([U-^{13}C]AmB) via development of an improved biosynthetic protocol[18]. By using uniformly ^{13}C-labeled glucose ([U-^{13}C]glucose) as the primary carbon source, we developed a robust procedure for attaining >80% ^{13}C incorporation, the highest ^{13}C enrichment yet reported for this natural product (**Supplementary Results**, **Supplementary Note**). This highly enriched [U-^{13}C]AmB enabled confident assignment of ^{13}C resonances and high sensitivity PRE measurements even at high lipid/AmB ratios.

We next identified a physiologically relevant lipid bilayer system in which we could execute the targeted experiments. Recent structure-function studies with AmB reveal that, in contrast to liposomes comprised of fully saturated lipids, liposomes derived from monounsaturated 1-palmitoyl-2-oleoyl-*sn*-glycero-3-phosphocholine (POPC) and Erg yield results that mirror those obtained with live yeast cells[25,27]. Also, unlike membranes derived from fully saturated lipids, the plasma membranes of yeast and bilayers derived from POPC-Erg are both in the liquid crystalline state at 23 °C[35,36]. In yeast, POPC is highly abundant, and Erg is the most common sterol[37]. Moreover, at the minimum inhibitory concentration for AmB against both *Saccharomyces cerevisiae* and *Candida albicans*, there is at least as much AmB as there is Erg[25]. We thus prepared lipid bilayer samples throughout this study with molar ratios of at least 10:1 POPC/Erg; for those samples containing AmB, we used at least 1 equiv. of AmB (relative to Erg). These bilayers showed proper phase behavior and retained this behavior in the presence of DOXYL spin labels (**Supplementary Fig. 1**).

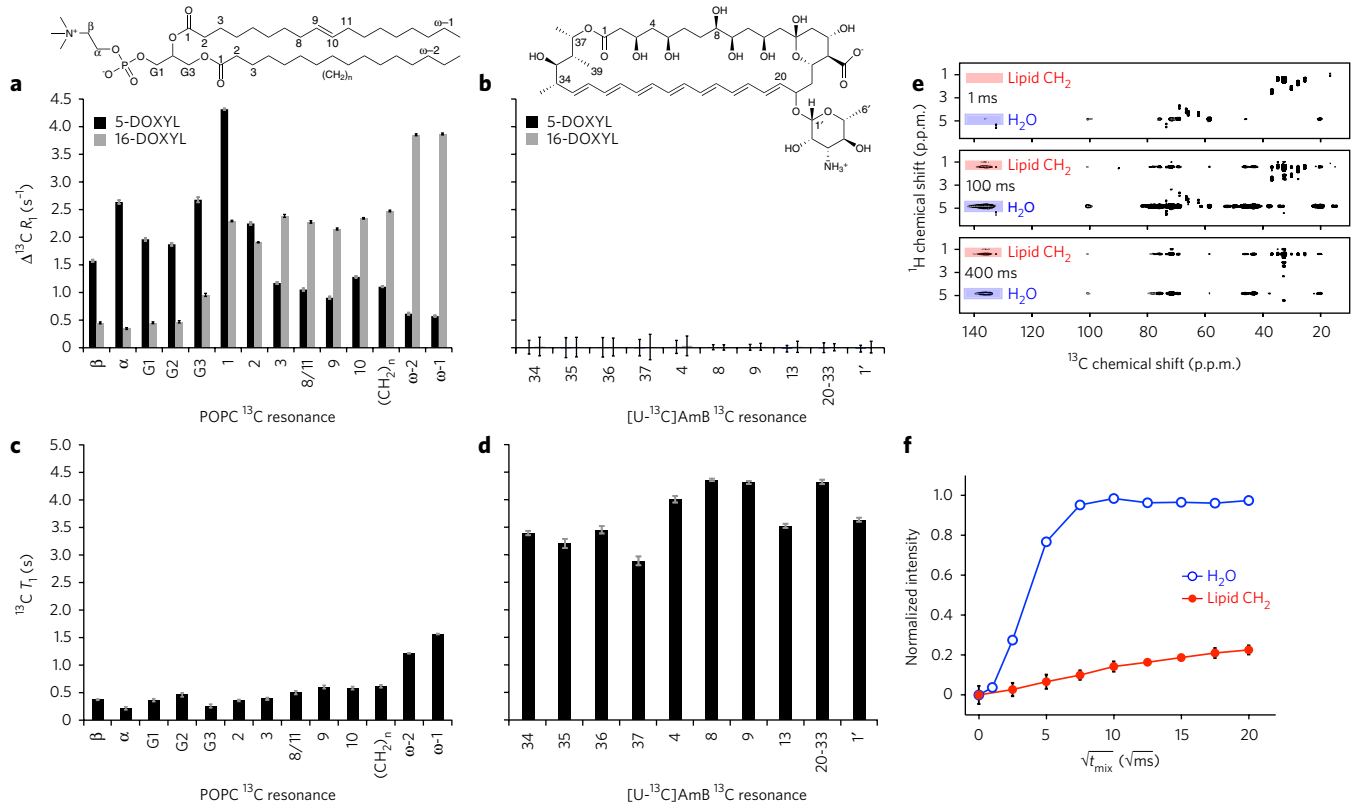

Figure 2 | AmB primarily exists as large extramembranous aggregates. (**a**) PRE values have magnitude proportional to $1/r^6$, where r is the distance from spin label to NMR-detected nucleus. POPC controls demonstrated this proportionality in the presence of 5 mol% 5-DOXYL-PC (black) or 16-DOXYL-PC (gray). (**b**) [U-^{13}C]AmB demonstrated no PRE effects ≥0.03 s^{-1} in the presence of either 5-DOXYL-PC (black) or 16-DOXYL-PC (gray) paramagnetic probes. (**c**,**d**) Substantial differences were observed between longitudinal (T_1) ^{13}C relaxation times for sites in POPC (**c**) and AmB (**d**). (**e**) Selected ^{1}H-^{13}C two-dimensional spectra were collected with a 1 ms T_2 filter and ^{1}H-^{1}H spin diffusion times of 1 ms, 100 ms and 400 ms; cross-peaks were from lipid acyl chains (red) and water (blue) to the [U-^{13}C]AmB polyene region. (**f**) The polarization transfer was quantified as a function of spin diffusion time from water and lipid to [U-^{13}C]AmB polyene. PRE values were derived from the difference between ^{13}C R_1 relaxation rates measured via inversion recovery for diamagnetic samples and samples containing 5-DOXYL-PC and 16-DOXYL-PC. Error bars were determined by χ^2 analysis. ^{1}H-^{13}C spin diffusion data were normalized relative to maximum intensity observed for both lipid and water cross-peaks for a given ^{13}C site after correcting for ^{1}H T_1 relaxation. Error bars were derived from the signal-to-noise ratio of the observed cross peak. Spectra were acquired at 14.1 T (600 MHz, ^{1}H frequency) at 20 °C, 10 kHz MAS.

To first confirm the position of each spin label in the bilayer, we determined the respective PRE values on ^{13}C resonances in natural abundance POPC lipids with 5 mol% of each DOXYL spin label (**Fig. 2a**). Consistent with the structure of POPC membranes[35], bilayers doped with 5% 16-DOXYL-PC demonstrated a maximal PRE at the termini of the POPC fatty acid chains, and the PRE decreased as the distance from the center of the membrane increased (**Fig. 2a**). The incorporation of 5-DOXYL-PC alternatively yielded maximal PRE values in the intermediate and head group regions of the lipid bilayer and much smaller, yet still readily observable, effects at the membrane interior. Thus, these two spin label probes enabled confident and complementary interrogation of the innermost and outermost regions of a lipid bilayer in a straightforward SSNMR experiment.

We next prepared samples with [U-^{13}C]AmB in POPC-Erg bilayers and used a series of ^{13}C chemical shift correlation experiments (including constant-time uniform-sign cross-peak correlation spectroscopy[38], dipolar-assisted rotational resonance[39] and supercycled POST-C5 recoupling[40]) to assign *de novo* the ^{13}C resonances of AmB (Online Methods, **Supplementary Figs. 2** and **3**, **Supplementary Table 1** and **Supplementary Note**). We then performed PRE measurements in the presence of 16-DOXYL-PC or 5-DOXYL-PC spin probes. The results were unambiguous. As predicted by the extramembranous sterol sponge model, and inconsistent with both the membrane-inserted ion channel and surface adsorption models, we observed no PRE values ≥0.03 s^{-1} to any ^{13}C resonances of AmB with either probe (**Fig. 2b**). Thus, the majority of AmB in these samples was >20 Å away from the membrane-embedded spin labels.

AmB primarily exists as large extramembranous aggregates

A series of additional SSNMR experiments further revealed that AmB exists in the form of large aggregates that are more closely associated with water than lipids. The longitudinal relaxation times (T_1 values) for AmB were substantially longer than those of the lipids, consistent with large and relatively immobile aggregates of AmB (**Fig. 2c**,**d** and **Supplementary Table 2**). SSNMR spin diffusion experiments, designed for the purpose of probing membrane protein topology[41], revealed that lipid-AmB correlations reached maximum intensity only at very long mixing times (~400 ms) for all resolvable carbons on AmB (**Fig. 2e**,**f** and **Supplementary Fig. 4**), indicating that the majority of the lipids were >15 Å away from the AmB. In contrast, we observed strong correlations between water and AmB within just 25 ms, consistent with intimate proximity of the AmB aggregates to water.

To further probe these aggregates and distinguish between an intramembranous vs. extramembranous location, we also performed TEM analysis of large unilamellar vesicles (LUVs) with the same ratio of POPC/Erg with or without AmB. In the absence of added AmB, we observed well-formed LUVs (**Fig. 3a** and **Supplementary Fig. 5a**).

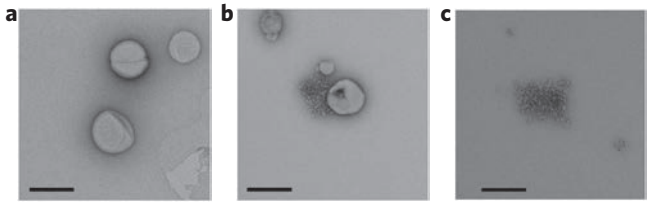

Figure 3 | Direct visualization of large extramembranous aggregates of AmB by TEM. (**a**) POPC/Erg 10:1 liposomes (**Supplementary Fig. 5a**). (**b**) POPC/Erg 10:1 liposomes with 1 equiv. (relative to Erg) of added AmB (**Supplementary Fig. 5b**). (**c**) AmB only (**Supplementary Fig. 5c**). Scale bars, 200 nm.

When AmB was added, we observed large extramembranous aggregates (**Fig. 3b** and **Supplementary Fig. 5b**). These aggregates were associated with one or more LUVs, suggesting an interaction between the surfaces of the aggregate and the lipid bilayer. When we added the same amount of AmB to the same volume of buffer devoid of LUVs, similar aggregates of AmB were observed (**Fig. 3c** and **Supplementary Fig. 5c**). These observations are consistent with the spontaneous formation in aqueous buffer of large AmB aggregates that externally associate with the surface of lipid bilayers.

Notably, parallel potassium efflux experiments revealed readily observable membrane permeabilization upon adding the same concentration of AmB to suspensions of the same POPC-Erg LUVs (**Supplementary Fig. 6**). This observation was consistent with a minor fraction of AmB existing in the form of membrane-permeabilizing ion channels that are too small to be visualized by TEM. This analysis was also consistent with all of our SSNMR data, in which the limits of detection permit up to 5% of the AmB existing in the membrane (Online Methods).

Extramembranous AmB aggregates extract Erg from bilayers

With the structural aspects of the sterol sponge model confirmed, we aimed to test the functional prediction that these large extramembranous aggregates of AmB extract Erg from lipid bilayers. We first performed a modified SSNMR PRE experiment in which we analyzed ^{13}C skip-labeled Erg ([^{13}C]Erg; **Fig. 4a**)[19] in spin label-containing bilayers as a function of AmB/[^{13}C]Erg ratio (**Fig. 4a**). This labeling pattern provided sufficient sensitivity that the ratio of POPC to Erg was increased to 40:1, readily enabling titrations of the AmB/Erg molar ratio while retaining the biophysical properties of the lipid bilayer. Thus, we prepared bilayers comprising POPC/[^{13}C]Erg at a 40:1 ratio ± 5 mol% 16-DOXYL without or with increasing amounts of natural abundance AmB. AmB had minimal effect on the POPC PRE (**Supplementary Fig. 7**). In contrast, we observed a progressive decrease in the [^{13}C]Erg PRE as the amount of AmB increased, indicating that Erg increasingly occupied a position outside the lipid bilayer (**Fig. 4a** and **Supplementary Fig. 7a**). In the absence of AmB (AmB/[^{13}C]Erg 0:1), we observed substantial PRE values for the resolved ^{13}C signals of [^{13}C]Erg; for several sites, such as Erg-18, Erg-21, Erg-22, Erg-24, Erg 26 and Erg-27, the PRE was ~1.5 s^{-1} or greater, and the ^{13}C T_1 values were relatively short (<1.5 s) (**Supplementary Fig. 7b**). These findings are consistent with the structure of Erg-containing membranes in which the Erg was inserted into the hydrophobic core of the bilayer[35], with the isopropyl tail most deeply inserted and therefore most proximate to the 16-DOXYL label. These conformation-specific PRE values for [^{13}C]Erg decreased markedly in the presence of AmB (**Fig. 4a** and **Supplementary Fig. 7a**). Specifically, with increasing amounts of natural abundance AmB (AmB/[^{13}C]Erg ratios of 1:1, 4:1 and 8:1), we observed a progressive decrease, with at least a threefold reduction in observed PRE in the AmB/[^{13}C]Erg 8:1 sample. These results support the interpretation that, in the presence of increasing amounts of AmB, Erg increasingly occupied a position outside the lipid bilayer membrane.

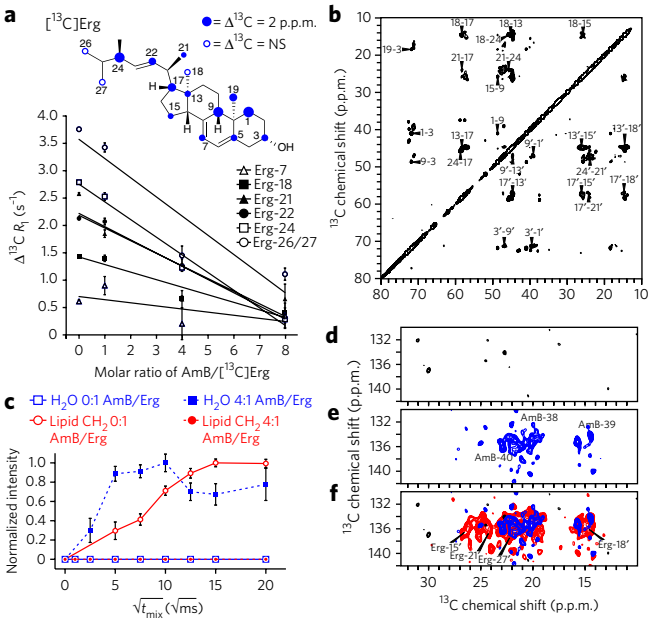

Figure 4 | AmB extracts Erg from lipid bilayers. (**a**) Samples prepared using 40:1 POPC/ [^{13}C]Erg ± 5 mol% 16-DOXYL-PC showed a progressive decrease in PRE effects of resolved Erg resonances as the ratio of AmB/[^{13}C]Erg increased. (**b**) The two-dimensional ^{13}C-^{13}C DARR spectrum of [^{13}C]Erg (250-ms mixing, 10:1:1 POPC/AmB/[^{13}C]Erg) changed in the presence of AmB, exhibiting new cross-peaks. (**c**) The ^{1}H-^{13}C polarization transfers from water (blue) and lipid (red) to Erg-7 were substantially different in the absence (closed circles and squares, dashed line) and presence (open circles and squares, solid line) of AmB. (**d**–**f**) Expansions of the olefin-to-methyl spectral region for two-dimensional [^{1}H]-^{13}C-[^{1}H-^{1}H]-^{13}C spectra[42,43] of only [^{13}C]Erg (328 h signal averaging time) (**d**), only [U-^{13}C]AmB (187 h) (**e**) and both [^{13}C]Erg and [U-^{13}C]AmB (187 h) (**f**). Error bars in **a** were derived from χ^2 analysis of inversion recovery trajectories. The ^{1}H-^{13}C spin diffusion data in **c** were normalized relative to the maximum intensity observed for both lipid and water cross-peaks for a given ^{13}C site after correcting for ^{1}H T_1 relaxation, and error bars were derived from the signal-to-noise of the observed cross-peak. Spectra were acquired at 14.1 T (600 MHz ^{1}H frequency). Data in **a**–**c** were acquired at 10 kHz MAS, at 20 °C and 10 °C, respectively. The [^{1}H]-^{13}C-[^{1}H-^{1}H]-^{13}C spectra (**d**–**f**) were acquired at 10 °C, 11.628 kHz MAS; processed with 40-Hz and 75-Hz line broadening in the direct and indirect dimensions, respectively; and were drawn with contour threshold set to four times the r.m.s. noise.

Additional SSNMR experiments also supported this conclusion and further demonstrated that the extracted Erg is physically bound to the extramembranous aggregates of AmB. As the ratio of AmB/[^{13}C]Erg increased, Erg resonances, but not those of POPC, demonstrated inhomogeneous broadening[19], consistent with a transition from a mobile state to an immobile state (**Supplementary Fig. 8** and **Supplementary Table 2**). The average ^{13}C T_1 relaxation values for [^{13}C]Erg also followed the expected trend, increasing with the AmB/[^{13}C]Erg ratio (**Supplementary Fig. 7b**). Two-dimensional ^{13}C-^{13}C correlation spectra further revealed several [^{13}C]Erg resonances that shifted by more than 0.4 p.p.m. in the presence of AmB (**Fig. 4b** and **Supplementary Table 3**), and resolved bound state resonances showed higher line width and T_1 values than those of the corresponding unbound state (**Supplementary Fig. 9**). In the absence of AmB, we observed very strong lipid-Erg correlations and no water-Erg correlations (**Fig. 4c** and **Supplementary Fig. 10**)[41], whereas in the presence of AmB we observed strong water correlations to all resolved Erg sites, with polarization transfer rates similar to those observed for AmB (**Fig. 4c** and **Supplementary**

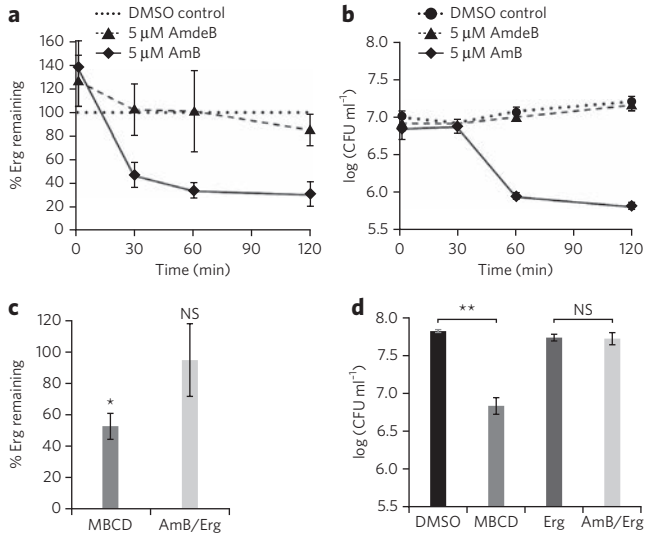

Figure 5 | AmB extracts Erg from and thereby kills yeast cells. (**a**) AmB extracted Erg from the membranes of *S. cerevisiae* cells in a time-dependent manner, whereas the non-Erg-binding derivative AmdeB showed no Erg-extracting activity. The percentage of Erg remaining in the cell membranes was normalized to that measured in DMSO-only treated controls. (**b**) Cell killing paralleled Erg extraction in AmB-treated cells. The non-Erg-extracting derivative AmdeB showed no cell-killing effects. (**c**) Erg extraction after 120 min of incubation. 500 mM MBCD extracted Erg from the membranes of *S. cerevisiae* cells, whereas a pre-formed 5 μM AmB/25 μM Erg complex did not. The percentage of Erg remaining in the cell membranes was normalized to that in DMSO-only and 25 μM Erg in DMSO-only treated controls, respectively. (**d**) Cell killing after 120 min incubation was observed for yeast treated with 500 mM MBCD but not for yeast treated with 5 μM AmB/25 μM Erg complex. Data represent mean ± s.e.m. for at least three independent experiments. $^{*}P < 0.02$; $^{**}P < 0.002$; NS, not significant.

Fig. 11). We also repeated one- and two-dimensional chemical shift, line width and T_1 analyses of [^{13}C]Erg in the presence of amphoteronolide B (AmdeB), a synthesized derivative of AmB that lacks the mycosamine appendage and does not bind Erg[25,27], and observed no [^{13}C]Erg chemical shift perturbations and only very small changes in line widths and T_1 values (**Supplementary Fig. 12**).

To definitively probe whether the extracted Erg is bound to the AmB aggregate, we prepared an additional series of samples in which ^{13}C labels were placed on (i) only Erg (**Fig. 4d**), (ii) only AmB (**Fig. 4e**) and (iii) both AmB and Erg (**Fig. 4f**). [^{1}H]-^{13}C-[^{1}H-^{1}H]-^{13}C spectra[42,43] for the first two samples showed only the anticipated intramolecular correlations (**Fig. 4d**,**e**), whereas the sample containing labels on both AmB and Erg revealed many new intermolecular AmB-Erg cross-peaks (**Fig. 4f**), consistent with Erg aligned parallel to the polyene region of AmB and directly confirming the formation of a small molecule–small molecule complex. We also measured the ^{1}H-^{13}C dipolar couplings for resolved sites in both AmB and Erg using the T-MREV recoupling sequence[44] (Online Methods and **Supplementary Fig. 13**) and Erg (**Supplementary Fig. 14**) to determine the relative mobility of these sites. In the absence of AmB, Erg was mobile, as evidenced by the low order parameters, but in the presence of AmB, the order parameters shifted to the same rigid lattice limit observed for AmB (**Supplementary Table 2**). Furthermore, we observed line widths of >110 Hz for both AmB and Erg in the sterol sponge (**Supplementary Table 2**). Thus, AmB extracts Erg from lipid bilayers into large, extramembranous aggregates.

AmB extracts Erg from and thereby kills yeast cells

Finally, we tested the validity of the sterol sponge model in cells. First, we probed whether AmB extracts Erg from the cell membrane of yeast by adapting an ultracentrifugation-based membrane isolation assay[45] to quantify the amount of Erg in the membranes of live *S. cerevisiae* cells in the absence and presence of AmB (Online Methods). AmB very effectively extracted Erg in a time-dependent fashion (**Fig. 5a**). In contrast, we observed no Erg-extracting effects with the non-Erg-binding derivative AmdeB.

Further experiments demonstrated that the Erg-extracting activity of AmB was responsible for its cell-killing effects. We observed no cell killing with DMSO or AmdeB (**Fig. 5b**), whereas AmB promoted robust cell killing with a time course that paralleled Erg extraction. In addition, methyl-β-cyclodextrin (MBCD), a cyclic oligosaccharide known to extract sterols from membranes[46], similarly demonstrated both Erg-extracting and cell-killing activities (**Fig. 5c**,**d**). Finally, the sterol sponge model predicts that AmB aggregates presaturated with Erg will lose the ability to extract Erg from membranes and kill yeast. Enabling this hypothesis to be tested, we found conditions that promoted the formation of stable and soluble aggregates of AmB and Erg (Online Methods). As predicted, treating cells with this preformed AmB–Erg complex resulted in no Erg extraction (**Fig. 5c**) and no cell killing (**Fig. 5d**).

DISCUSSION

For decades, scientists have widely accepted that membrane-spanning ion channels primarily contribute to the structure and antifungal activity of AmB (**Fig. 1b**)[4–23]. In contrast, we found that AmB primarily forms large extramembranous aggregates that extract Erg from lipid bilayers and thereby kill yeast. Membrane-inserted ion channels are relatively minor contributors, both structurally and functionally, to the antifungal action of this natural product. Although previous studies have reported large aggregates of AmB or its derivatives[17,21], the interpretation of these findings has been in terms of the ion channel model. Here we described PRE (**Fig. 2b**,**d**), ^{1}H spin diffusion trajectory (**Figs. 2f** and **4c** and **Supplementary Figs. 4**, **10** and **11**) and TEM studies (**Fig. 3a–c** and **Supplementary Fig. 5**) that collectively demonstrated that AmB primarily exists in the form of large extramembranous aggregates. Moreover, changes in PRE values, ^{1}H spin diffusion trajectories, T_1 relaxation, order parameters, line widths and chemical shift perturbations as well as the observation of direct intermolecular cross-peaks and the results of cell-based Erg extraction experiments demonstrated that extramembranous aggregates of AmB directly bind Erg. We further confirmed that the AmB aggregates we observed in our SSNMR, TEM and cell-based experiments were similar (**Supplementary Fig. 15**). Collectively, these results strongly support the proposed sterol sponge model in which extramembranous aggregates of AmB extract Erg from phospholipid bilayers and thereby kill yeast.

The sterol sponge model provides a new foundation for better understanding and more effectively harnessing the unique biophysical, biological and medicinal properties of this small-molecule natural product. Many efforts over the past several decades that were based on the classic ion channel model to improve the therapeutic index of AmB focused on selectively permeabilizing yeast versus human cells[11,13]. This approach has not yielded a clinically viable derivative of the natural product. The sterol sponge model suggests that an alternative approach will be more effective. Specifically, analogous to the now-clarified mechanism of antifungal activity, the extraction of cholesterol by large extramembranous aggregates of AmB may be primarily responsible for toxicity to human cells. This, in turn, suggests that the goal should be to maximize the relative binding affinity of AmB aggregates for Erg versus cholesterol. This insight is already guiding development of the first derivatives of AmB that are toxic to yeast cells but not human cells and thus hold exceptional promise for yielding an improved therapeutic index[47].

A high-resolution structure of the large, extramembranous AmB aggregate, with and without bound Erg and cholesterol, would

powerfully enable the discovery and/or further development of such derivatives. Notably, the results described herein provide a strong platform for determining such a structure. Specifically, the large extramembranous aggregate of AmB, confirmed to reproducibly and stably form in the presence of POPC bilayers (**Supplementary Figs. 2** and **15**), represents an excellent substrate for SSNMR analysis, and the common relaxation properties of AmB and Erg are consistent with the existence of a stable complex. Moreover, the two-dimensional [^{1}H]-^{13}C-[^{1}H-^{1}H]-^{13}C spectra of the complex derived from [U-^{13}C]AmB and [^{13}C]Erg (**Fig. 4f**) showed intermolecular AmB-Erg correlations with intensities indicating internuclear distances of ~6 Å or less. We further note that comparison of ^{13}C-^{13}C two-dimensional spectra of 10:1:0 POPC/[U-^{13}C]AmB/Erg and 10:1:1 POPC/[U-^{13}C]AmB/Erg (**Supplementary Fig. 2**) showed that the structures of the AmB aggregates in the absence and presence of Erg were very similar. There were, however, some intriguing changes in the AmB resonances corresponding to the mycosamine appendage upon the binding of Erg (**Supplementary Fig. 3**), which will be the subject of future investigations.

We anticipate that further SSNMR studies, including those applied to derivatives of AmB and Erg or cholesterol with site-specific or skip-pattern isotopic labels, will enable us to define in high resolution the structure of this extramembranous aggregate and the interface between these small molecules. Such information may reveal the structural underpinnings of the small preference of AmB to bind Erg over cholesterol and further guide the development of derivatives of AmB that maximize this binding preference and thus the therapeutic index[47]. In this vein, we note that the pattern of chemical shift perturbations observed for Erg in the absence and presence of AmB are consistent with tight association between AmB and the A and B rings of the sterol. Remarkably, the B ring of cholesterol, to which AmB binds but less strongly than Erg[27,47], is more sterically bulky than that of Erg because it has an extra degree of saturation. Moreover, lanosterol, to which AmB does not bind[27], has both the same extra degree of saturation in the B ring and a sterically bulky gem dimethyl group on the A ring. Although further studies are required to provide a detailed picture, our current data begin to support a structural rationale for the differential binding of AmB to Erg (strong), cholesterol (weak) and lanosterol (no binding). More broadly, relative to small molecules that bind proteins, small molecules that bind other small molecules in a biologically relevant fashion are very rare. A high-resolution structure of this prototypical AmB–Erg complex may enable rational pursuit and study of other biologically important small molecule–small molecule interactions.

The sterol sponge model also offers a new rationale for the paucity of clinically relevant microbial resistance that is a hallmark of AmB as a therapeutic. Because the extraction of Erg renders yeast membranes Erg deficient, AmB may simultaneously perturb all of the cellular processes that depend on membrane Erg[28–31,48]. This most likely includes many different membrane proteins that directly bind Erg[28–31], and simultaneous mutation of all such proteins in a manner that alleviates this Erg dependence is highly improbable. It has also remained unclear why, in contrast to the rarity with which AmB-resistant mutants are found in patients, it is relatively easy to generate AmB-resistant yeast mutants in cell culture experiments[49]. The sterol sponge model provides a rationale for this dichotomy. AmB-resistant mutants generated in cell culture generally have modified sterols in their membranes, for example, lanosterol[50] (and/or other biosynthetic precursors to Erg), to which AmB does not bind (described above)[27]. It was previously assumed that such changes in sterol content minimize antifungal potency by minimizing membrane-permeabilizing activity[9,10,13,49]. The sterol sponge model alternatively suggests that, because AmB does not bind or extract lanosterol, this modified sterol remains in the membrane to serve as a surrogate binding partner for sterol-dependent proteins. Owing to the structural differences between lanosterol and Erg described above, however, the former is most likely only a minimally effective substitute, resulting in reduced activity of many proteins that require specific interactions with Erg to function properly. This, in turn, may translate into substantially reduced pathogenicity of the resulting yeast mutants. Consistent with this notion, strains of yeast with modified sterol content have markedly reduced pathogenicity in animal models[49]. Such strains may routinely emerge in patients treated with AmB, but, owing to their reduced pathogenicity, cannot thrive and/or are rapidly cleared by the immune system of the host. A recently reported alternative series of studies provide complementary support for these conclusions[49].

The clarified picture of the structural and functional underpinnings of AmB activity provided by the sterol sponge model also illuminates a rational road map for separating the ion channel forming and cytotoxic activities of AmB. Small, membrane-spanning ion channel aggregates most likely exist as minor components in equilibrium with the large extramembranous assemblies of AmB characterized herein. This proposal is consistent with the weak AmB-lipid correlations observed in the SSNMR spin diffusion experiments and the limits of detection of the SSNMR PRE and TEM studies. As we have previously demonstrated, binding Erg in the absence of channel activity is sufficient for cell killing[25]. Specifically, the capacity for channel formation can be selectively eliminated while preserving the capacity for both Erg binding and cell killing by deleting the C35 hydroxyl group appended to AmB[25]. In the sterol sponge model, this result can be rationalized by invoking a selectively destabilizing influence of this functional group deletion on the smaller membrane-inserted channel aggregates. Future studies will aim to determine whether this putative equilibrium between large extramembranous and small membrane-spanning aggregates can be alternatively shifted to favor ion channel formation, thereby maximizing potentially useful membrane-permeabilizing functions[25] while minimizing cytotoxic sterol extracting activity.

In summary, for more than half a century, the classic ion channel model has dominated the conceptual framework through which scientists have perceived and studied the structure and function of AmB in lipid bilayers. In contrast to this classic model, AmB primarily exists in the form of large, extramembranous aggregates that physically extract Erg from lipid bilayers and thereby kill yeast. This new sterol sponge model stands to more effectively guide the understanding, optimization and clinical use of this prototypical small-molecule natural product as well as other small molecules that similarly interface with living systems.

Received 19 August 2013; accepted 20 February 2014;
published online 30 March 2014

METHODS

Methods and any associated references are available in the online version of the paper.

References

1. Cannon, R.D. *et al. Candida albicans* drug resistance—another way to cope with stress. *Microbiology* **153**, 3211–3217 (2007).
2. Mora-Duarte, J. *et al.* Comparison of caspofungin and amphotericin B for invasive candidiasis. *N. Engl. J. Med.* **347**, 2020–2029 (2002).
3. Monk, B.C. & Goffeau, A. Outwitting multidrug resistance to antifungals. *Science* **321**, 367–369 (2008).
4. Ermishkin, L.N., Kasumov, K.M. & Potzeluyev, V.M. Single ionic channels induced in lipid bilayers by polyene antibiotics amphotericin-B and nystatine. *Nature* **262**, 698–699 (1976).
5. Andreoli, T.E. & Monahan, M. The interaction of polyene antibiotics with thin lipid membranes. *J. Gen. Physiol.* **52**, 300–325 (1968).
6. Cass, A., Finkelstein, A. & Krespi, V. The ion permeability induced in thin lipid membranes by the polyene antibiotics nystatin and amphotericin B. *J. Gen. Physiol.* **56**, 100–124 (1970).
7. Finkelstein, A. & Holz, R. Aqueous pores created in thin lipid membranes by the polyene antibiotics nystatin and amphotericin B. *Membranes* **2**, 377–408 (1973).

8. Andreoli, T.E. Structure and function of amphotericin B–cholesterol pores in lipid bilayer membranes. *Ann. NY Acad. Sci.* **235**, 448–468 (1974).
9. de Kruijff, B. & Demel, R.A. Polyene antibiotic-sterol interactions in membranes of *Acholeplasma laidlawii* cells and lecithin liposomes. III. Molecular structure of polyene antibiotic–cholesterol complexes. *Biochim. Biophys. Acta* **339**, 57–70 (1974).
10. Bolard, J. How do the polyene macrolide antibiotics affect the cellular membrane-properties. *Biochim. Biophys. Acta* **864**, 257–304 (1986).
11. Volmer, A.A., Szpilman, A.M. & Carreira, E.M. Synthesis and biological evaluation of amphotericin B derivatives. *Nat. Prod. Rep.* **27**, 1329–1349 (2010).
12. Cereghetti, D.M. & Carreira, E.M. Amphotericin B: 50 years of chemistry and biochemistry. *Synthesis* **2006**, 914–942 (2006).
13. Chéron, M. *et al.* Quantitative structure-activity relationships in amphotericin B derivatives. *Biochem. Pharmacol.* **37**, 827–836 (1988).
14. Croatt, M.P. & Carreira, E.M. Probing the role of the mycosamine C2′-OH on the activity of amphotericin B. *Org. Lett.* **13**, 1390–1393 (2011).
15. Baginski, M., Resat, H. & Borowski, E. Comparative molecular dynamics simulations of amphotericin B–cholesterol/ergosterol membrane channels. *Biochim. Biophys. Acta* **1567**, 63–78 (2002).
16. Murata, M. *et al.* Ion channel complex of antibiotics as viewed by NMR. *Pure Appl. Chem.* **81**, 1123–1129 (2009).
17. Matsumori, N., Sawada, Y. & Murata, M. Large molecular assembly of amphotericin B formed in ergosterol-containing membrane evidenced by solid-state NMR of intramolecular bridged derivative. *J. Am. Chem. Soc.* **128**, 11977–11984 (2006).
18. Matsuoka, S. *et al.* Membrane interaction of amphotericin B as single-length assembly examined by solid state NMR for uniformly ^{13}C-enriched agent. *Bioorg. Med. Chem.* **14**, 6608–6614 (2006).
19. Umegawa, Y. *et al.* Head-to-tail interaction between amphotericin B and ergosterol occurs in hydrated phospholipid membrane. *Biochemistry* **51**, 83–89 (2012).
20. Verkleij, A.J. *et al.* Freeze-etch electron microscopy of erythrocytes, *Acholeplasma laidlawii* cells and liposomal membranes after action of filipin and amphotericin B. *Biochim. Biophys. Acta* **291**, 577–581 (1973).
21. Milhaud, J., Ponsinet, V., Takashi, M. & Michels, B. Interactions of the drug amphotericin B with phospholipid membranes containing or not ergosterol: new insight, into them role of ergosterol. *Biochim. Biophys. Acta* **1558**, 95–108 (2002).
22. Mouri, R. *et al.* Complex formation of amphotericin B in sterol-containing membranes as evidenced by surface plasmon resonance. *Biochemistry* **47**, 7807–7815 (2008).
23. Katzung, B.G., Masters, S.B. & Trevor, A.J. *Basic and Clinical Pharmacology* 12th edn. (McGraw-Hill Education, Europe, 2012).
24. Fernandez-Lopez, S. *et al.* Antibacterial agents based on the cyclic D,L-α-peptide architecture. *Nature* **412**, 452–455 (2001).
25. Gray, K.C. *et al.* Amphotericin primarily kills yeast by simply binding ergosterol. *Proc. Natl. Acad. Sci. USA* **109**, 2234–2239 (2012).
26. Palacios, D.S., Anderson, T.M. & Burke, M.D. A post-PKS oxidation of the amphotericin B skeleton predicted to be critical for channel formation is not required for potent antifungal activity. *J. Am. Chem. Soc.* **129**, 13804–13805 (2007).
27. Palacios, D.S. *et al.* Synthesis-enabled functional group deletions reveal key underpinnings of amphotericin B ion channel and antifungal activities. *Proc. Natl. Acad. Sci. USA* **108**, 6733–6738 (2011).
28. Jin, H., McCaffery, J.M. & Grote, E. Ergosterol promotes pheromone signaling and plasma membrane fusion in mating yeast. *J. Cell Biol.* **180**, 813–826 (2008).
29. Kato, M. & Wickner, W. Ergosterol is required for the Sec18/ATP-dependent priming step of homotypic vacuole fusion. *EMBO J.* **20**, 4035–4040 (2001).
30. Heese-Peck, A. *et al.* Multiple functions of sterols in yeast endocytosis. *Mol. Biol. Cell* **13**, 2664–2680 (2002).
31. te Welscher, Y.M. *et al.* Polyene antibiotic that inhibits membrane transport proteins. *Proc. Natl. Acad. Sci. USA* **109**, 11156–11159 (2012).
32. Solomon, I. Relaxation processes in a system of 2 spins. *Phys. Rev.* **99**, 559–565 (1955).
33. Nadaud, P.S., Helmus, J.J., Hofer, N. & Jaroniec, C.P. Long-range structural restraints in spin-labeled proteins probed by solid-state nuclear magnetic resonance spectroscopy. *J. Am. Chem. Soc.* **129**, 7502–7503 (2007).
34. Sankaram, M.B. & Thompson, T.E. Cholesterol-induced fluid-phase immiscibility in membranes. *Proc. Natl. Acad. Sci. USA* **88**, 8686–8690 (1991).
35. Hsueh, Y.W. *et al.* Ergosterol in POPC membranes: physical properties and comparison with structurally similar sterols. *Biophys. J.* **92**, 1606–1615 (2007).
36. Watson, K., Bertoli, E. & Griffiths, D.E. Phase transitions in yeast mitochondrial membranes—effect of temperature on energies of activation of respiratory enzymes of *Saccharomyces cerevisiae*. *Biochem. J.* **146**, 401–407 (1975).
37. Ejsing, C.S. *et al.* Global analysis of the yeast lipidome by quantitative shotgun mass spectrometry. *Proc. Natl. Acad. Sci. USA* **106**, 2136–2141 (2009).
38. Chen, L. *et al.* Constant-time through-bond ^{13}C correlation spectroscopy for assigning protein resonances with solid-state NMR spectroscopy. *J. Am. Chem. Soc.* **128**, 9992–9993 (2006).
39. Takegoshi, K., Nakamura, S. & Terao, T. ^{13}C-^{1}H dipolar-assisted rotational resonance in magic-angle spinning NMR. *Chem. Phys. Lett.* **344**, 631–637 (2001).
40. Hohwy, M., Rienstra, C.M., Jaroniec, C.P. & Griffin, R.G. Fivefold symmetric homonuclear dipolar recoupling in rotating solids: application to double quantum spectroscopy. *J. Chem. Phys.* **110**, 7983–7992 (1999).
41. Huster, D., Yao, X.L. & Hong, M. Membrane protein topology probed by ^{1}H spin diffusion from lipids using solid-state NMR spectroscopy. *J. Am. Chem. Soc.* **124**, 874–883 (2002).
42. Lange, A., Luca, S. & Baldus, M. Structural constraints from proton-mediated rare-spin correlation spectroscopy in rotating solids. *J. Am. Chem. Soc.* **124**, 9704–9705 (2002).
43. Tang, M., Waring, A.J. & Hong, M. Intermolecular packing and alignment in an ordered beta-hairpin antimicrobial peptide aggregate from 2D solid-state NMR. *J. Am. Chem. Soc.* **127**, 13919–13927 (2005).
44. Hohwy, M. *et al.* Local structure and relaxation in solid-state NMR: Accurate measurement of amide N-H bond lengths and H-N-H bond angles. *J. Am. Chem. Soc.* **122**, 3218–3219 (2000).
45. Haas, A. A quantitative assay to measure homotypic vacuole fusion *in vitro*. *Methods Cell Sci.* **17**, 283–294 (1995).
46. Yancey, P.G. *et al.* Cellular cholesterol effect mediated by cyclodextrins—demonstration of kinetic pools and mechanism of efflux. *J. Biol. Chem.* **271**, 16026–16034 (1996).
47. Wilcock, B.C., Endo, M.M., Uno, B.E. & Burke, M.D. C2′-OH of amphotericin B plays an important role in binding the primary sterol of human cells but not yeast cells. *J. Am. Chem. Soc.* **135**, 8488–8491 (2013).
48. Kang, C.K. *et al.* Visualization analysis of the vacuole-targeting fungicidal activity of amphotericin B against the parent strain and an ergosterol-less mutant of *Saccharomyces cerevisiae*. *Microbiology* **159**, 939–947 (2013).
49. Vincent, B.M. *et al.* Fitness trade-offs restrict the evolution of resistance to amphotericin B. *PLoS Biol.* **11**, e1001692 (2013).
50. Sanglard, D. *et al. Candida albicans* mutations in the ergosterol biosynthetic pathway and resistance to several antifungal agents. *Antimicrob. Agents Chemother.* **47**, 2404–2412 (2003).

Acknowledgments

We gratefully acknowledge P.J. Hergenrother and E. Oldfield for helpful discussions, and we thank J.J. Lopez for preliminary spin diffusion SSNMR experiments. Portions of this work were supported by the US National Institutes of Health (NIH) (R01GM080436 and F30DK081272) and the University of Illinois at Urbana-Champaign (Centennial Scholar Award to C.M.R.). M.D.B. is a Howard Hughes Medical Institute Early Career Scientist. M.C.C. is an American Heart Association Predoctoral Fellow. T.M.A. is a Ruth L. Kirchstein NIH National Research Service Award Predoctoral Fellow. The Gonen lab is funded by the Howard Hughes Medical Institute.

Author contributions

T.M.A., M.C.C., A.G.C., K.A.D., A.J.N., G.C., T.G., C.M.R. and M.D.B. designed research. T.M.A., N.M. and A.G.C. prepared [U-^{13}C]AmB and [^{13}C]Erg. T.M.A., M.C.C., A.G.C., G.S.H., A.J.N., G.C. and B.E.U. prepared samples for SSNMR. M.C.C., A.J.N., G.C., G.S.H., M.D.T. and C.M.R. acquired SSNMR data. A.G.C. and T.G. performed microscopy. K.A.D. performed cell-based assays. T.M.A., M.C.C., A.G.C., K.A.D., G.S.H., M.D.T., A.J.N., G.C., S.W., B.E.U., E.L.W., T.G., C.M.R. and M.D.B. analyzed data. T.M.A., M.C.C., A.G.C., K.A.D., C.M.R. and M.D.B. wrote the paper.

Competing financial interests

The authors declare no competing financial interests.

Additional information

Supplementary information is available in the online version of the paper. Reprints and permissions information is available online at http://www.nature.com/reprints/index.html. Correspondence and requests for materials should be addressed to C.M.R. or M.D.B.

ONLINE METHODS

General methods. *Materials.* Commercially available materials were purchased from Sigma-Aldrich, Alfa Aesar, Avanti Polar Lipids, Cambridge Isotope Laboratories or Fisher Scientific and were used without further purification unless stated otherwise. Natural abundance AmB was purchased from Sigma-Aldrich or was a gift from the Bristol-Myers Squibb Company. Unless stated otherwise, all of the solvents were dispensed from a solvent purification system that passes solvents through packed columns according to the method described in ref. 52 (THF, Et_2O, CH_2Cl_2, toluene, dioxane, hexanes: dry neutral alumina; DMSO, DMF, CH_3OH: activated molecular sieves). Water was dispensed from a MilliQ water purification system (Millipore Corporation, Billerica, MA).

Purification and analysis. Preparative-scale HPLC purification was performed using an Agilent 1260 series instrument equipped with a multiple-wavelength detector and a Waters SunFire Prep C18 OBD 5 µm 30 × 150 mm column at a flow rate of 25 ml/min. All HPLC solvents were filtered through 0.2-µm Millipore filters before use. UV-vis analyses were performed on a Shimadzu PharmaSpec UV-1700 spectrophotometer. ESI-MS spectra were obtained at the University of Illinois mass spectrometry facility.

Amphotericin and AmdeB. Owing to the light and air sensitivity of polyenes, all of manipulations of AmB and AmdeB were carried out under low-light conditions, and compounds were stored under a dry argon atmosphere at −20 °C. AmdeB was prepared synthetically from natural abundance AmB as previously described[25–27]. All of the AmB and AmdeB used for current experiments were purified by preparative-scale HPLC. All manipulations of HPLC-purified AmB and AmdeB were performed using either Optima MeOH, 0.2-µm-filtered HPLC-grade solvents or solvents dispensed from a solvent purification system[52].

For purification, solid AmB was dissolved in DMSO (10 mg/ml), filtered through Celite 545 and purified (100-µl injections) with a gradient of 5% to 65% MeCN/5 mM ammonium acetate (NH_4OAc) over 12 min, with detection at 406 nm. The column was subsequently flushed with isocratic 95% MeCN/5 mM NH_4OAc for 2 min and re-equilibrated to 5% MeCN/5 mM NH_4OAc before the next injection. The combined AmB solution was concentrated *in vacuo* with filtered (0.2 µm) MeCN added back to the flask as needed for azeotropic removal of water. The resulting yellow solid was suspended via bath sonication in 1:1 MeCN/toluene and again concentrated *in vacuo* for azeotropic removal of residual NH_4OAc. Residual solvent was removed under high vacuum for ≥8 h to furnish a pale yellow solid, which was stored under argon at −20 °C.

AmdeB was dissolved in DMF, filtered (Celite 545), injected and eluted with a mobile phase gradient of 5% to 95% MeCN/5 mM NH_4OAc over 25 min.

Biosynthesis of [U-^{13}C]AmB. [U-^{13}C]AmB was prepared using a modified version of the method previously reported[18], with [U-^{13}C]glucose replacing natural abundance fructose in the culture medium. All simple carbon sources were thus uniformly ^{13}C labeled, resulting in unprecedented isotopic enrichment of >80%, as measured by MS. After workup and precipitation, [U-^{13}C]AmB was purified by gradient C18 chromatography followed by HPLC (**Supplementary Note**).

Erg. Natural abundance Erg was purchased from Sigma-Aldrich and recrystallized from EtOH before use. Stock solutions of 4 mg/ml Erg in $CHCl_3$ were stored under argon at −20 °C for up to 1 month. [^{13}C]Erg was prepared biosynthetically using the method previously described[19,51].

I. Solid-state NMR spectroscopy. SSNMR experiments were performed using a 600 MHz InfinityPlus spectrometer (Varian, now a subsidiary of Agilent Technologies, Inc.) equipped with a 3.2-mm T3 HXY MAS probe tuned to ^{1}H-^{31}P-^{13}C mode. Pulse widths (π/2) for ^{1}H, ^{13}C and ^{31}P were 2–2.5 µs, 3.2 µs and 3.2 µs, respectively. Spinning was controlled with a Varian MAS controller to 10,000 ± 2 Hz. SPINAL-64 decoupling (~75–80 kHz) was used during evolution and acquisition periods[53]. The flow rate of sample cooling gas was maintained at 100 standard cubic feet per hour (scfh) at 20 °C, resulting in a calibrated sample temperature of 19.2 ± 1 °C. Chemical shifts were referenced externally with adamantane, with the downfield ^{13}C resonance referenced to 40.48 p.p.m.[54].

^{13}C T_1 and PRE Experiments. T_1 values were measured using standard T_1 inversion recovery pulse sequence with a 5-s pulse delay. Data were processed and fit with Varian Spinsight software version 4.3.2. For each of the resolved methine and methylene in [U-^{13}C]amphotericin ([U-^{13}C]AmB) and [^{13}C]Erg, the longitudinal ^{13}C PRE was obtained by calculating the difference between the ^{13}C R_1 values for sample with and without 5 mol% of the DOXYL lipids, determined by modeling the individual relaxation trajectories as single exponential decays. T_1 trajectories were fit using the integrated volume of a given peak as a function of delay time (tau_1); integration boundaries were set to the line width at half-height. The average line widths were ~40–60 Hz for POPC, ~50 Hz for Erg with no AmB present, 127 Hz with AmB present (**Supplementary Table 3**) and ~187 Hz for AmB alone.

^{1}H-^{13}C spin-diffusion experiments. We performed ^{1}H-^{13}C spin-diffusion correlation experiments as previously described[41] using a 1-ms T_2 filter to detect interactions between the mobile ^{1}H signals of lipid acyl chains (1.35 p.p.m.) and/or water (4.7 p.p.m.) with [U-^{13}C]AmB and [^{13}C]Erg in the presence and absence of AmB. ^{1}H-^{13}C polarization transfer trajectories were extracted from ^{1}H-^{13}C two-dimensional spectra collected with ^{1}H-^{13}C mixing times ranging from 1 ms to 625 ms by fitting peaks with a minimum signal to noise of 5, using a box integration method in Sparky. Trajectories were then normalized on the basis of maximum observed intensity for a single resolved water or lipid ^{1}H-^{13}C cross peak after correction for ^{1}H T_1 relaxation, which was measured in a separate T_1 inversion recovery experiment. Error bars are derived from the signal-to-noise ratios observed for each cross-peak.

Order parameters from ^{1}H-^{13}C dipolar couplings. Dipolar order parameters (S) were measured using the T-MREV pulse sequence[44] at an MAS rate of 8.333 kHz (N = 4 condition, 100-kHz ^{1}H decoupling nutation frequency, 2.5-µs ^{1}H π/2 pulse length). The T-MREV ^{13}C-^{1}H dephasing had 30-µs increments, and a total of 25 increments were recorded in t_1. Fortran fitting routines[55] were used to determine the ^{13}C-^{1}H dipolar coupling, taking into account the effects of relaxation and contributions from weaker couplings from neighboring protons. We calibrated the scaling factor of the T-MREV sequence by measuring the ^{13}C-^{1}H dipolar couplings for crystalline *N*-acetyl-L-valine under the identical experimental conditions.

[^{1}H]-^{13}C-[^{1}H-^{1}H]-^{13}C correlation spectra. [^{1}H]-^{13}C-[^{1}H-^{1}H]-^{13}C SSNMR experiments were performed at 10 °C at an MAS rate 11.628 kHz, with the heteronuclear contact time (t_{HC}) set to 400 µs and a ^{1}H-^{1}H mixing time of 400 µs. These conditions reveal cross-peaks for internuclear ^{13}C-^{13}C distances of ~4–6 Å. To properly identify new intermolecular AmB-Erg cross-peaks, the [^{1}H]-^{13}C-[^{1}H-^{1}H]-^{13}C spectra were acquired back-to-back under identical conditions, including signal averaging, with adjustment of total measurement time on the basis of the amount of material. The rotors of POPC/[U-^{13}C]AmB/Erg (10:1:1 molar ratio) and POPC/U-^{13}C -AmB/[^{13}C]Erg (10:1:1 molar ratio) were packed with ~25 mg, and the spectra signal was averaged for 7.8 d each. The 10:1:1 POPC/AmB/[^{13}C]Erg sample was ~16 mg and therefore was signal averaged for 13.6 d. The three spectra were all processed identically, with 40-Hz and 75-Hz ^{13}C line broadening applied in the direct and indirect dimensions, respectively.

II. Preparation of samples for SSNMR. *Preparation of stock solutions.* A fresh stock solution of HPLC-purified AmB (natural abundance or [U-^{13}C]AmB) was prepared for each experiment by dissolving AmB in a large volume of Optima methanol, typically 75–100 ml for 10 mg of AmB. Stock solution concentration was measured in triplicate by dilution in MeOH and measuring absorbance at 406 nm (ε_{406} = 146,000 M^{-1} cm^{-1})[26].

Stock solutions of Erg were prepared by dissolving recrystallized (commercial) or HPLC-purified (biosynthetic) Erg in a minimum volume of $CHCl_3$, and the concentration was determined by UV-vis spectroscopy (ε_{282} = 10,400 M^{-1} cm^{-1})[27]. Erg stock solutions were stored in I-Chem vials under a dry argon atmosphere at −20 °C for up to 1 month.

Phospholipids were purchased as stock solutions in $CHCl_3$, and these solutions were used directly for liposome preparation. Unused phospholipid solutions were stored in vials or bottles under a dry argon atmosphere at −20 °C and discarded after 1 month.

Preparation of liposome vesicles for SSNMR. Liposomes were prepared using a modified version of the protocol previously reported.[18] A suspension of POPC/Erg/AmB in 1:1 $CHCl_3$/MeOH was prepared as follows: the desired amount of AmB stock solution (typically 30–40 ml) was concentrated *in vacuo* to 2–3 ml and transferred to a 7-ml Wheaton vial, with three Optima MeOH washes to ensure complete transfer. This resulting AmB suspension was concentrated *in vacuo*. The desired amounts of stock solutions of phospholipid and Erg were then added via Hamilton gastight syringe, and an equivalent volume of Optima MeOH was added to resuspend the AmB. The vial was

capped, and this suspension was briefly vortexed and bath-sonicated until no AmB remained adherent to the sides of the vial (2–3 cycles). Solvent was removed under a gentle stream of nitrogen gas. Residual solvent was removed under high vacuum for ≥8 h.

To the dried solid was added filter-sterilized 0.3 mM HEPES buffer, pH 7.0, to yield a final phospholipid concentration of 40 mM. This aqueous suspension was vortexed and sonicated three times or until a homogeneous suspension was observed. Samples were then submitted to five freeze-thaw cycles (liquid nitrogen and lukewarm tap water). Samples were again frozen in liquid nitrogen and lyophilized for ≥8 h. The lyophilization chamber was then back-filled with dry argon to prevent samples from absorbing ambient water. Samples were immediately capped and packed into rotors for SSNMR as soon as possible.

Dry samples were packed in 3.2-mm-diameter limited-speed SSNMR rotors (Agilent Technologies, Inc.) and hydrated with 8–10 µl of MilliQ H_2O. Rubber discs were used in the rotors to maintain hydration levels by creating a seal. Samples were placed at 4 °C for at least 24 h to allow water to equilibrate.

III. Electron microscopy. *General information.* LUVs were prepared by the method reported previously[25,27], and AmB was added to the LUV suspension as a freshly prepared DMSO stock solution. Microscopy was performed using a 120-keV FEI Spirit transmission electron microscope. Images were recorded using a bottom-mount TVIPS CMOS-based camera system at nominal magnifications of 23,000–49,000× at the specimen level. Measurements were taken in ImageJ32 (v 1.47).

Sample preparation. AmB was prepared as a stock DMSO solution (8.82 mM). 5 µl of the stock AmB solution was added to 95 µl of the 50× diluted LUV solutions. For AmB-free samples, 5 µl of DMSO was added to 95 µl of the 50× diluted LUV solutions. Samples were vortexed gently for 5 s and then incubated at 37 °C for 1 h. EM samples were prepared as previously described[56] with the following modifications: a 4-µl drop of the sample was applied to a negatively charged carbon-coated copper grid (Gilder 200 mesh, Ted Pella, Inc., Redding CA) for 30 s. Subsequently, two drops of freshly prepared 2% uranyl acetate were added to the sample and incubated for 1 min before drying via aspiration. Samples were then screened on the electron microscope.

IV. *In vivo* sterol extraction and membrane isolation. *Growth conditions for S. cerevisiae. S. cerevisiae* was grown in autoclave-sterilized yeast peptone dextrose (YPD) medium consisting of 10 g/l yeast extract, 20 g/l peptone and 20 g/l of filter-sterilized dextrose added as a sterile 40% w/v solution in water. Solid medium was prepared by pouring sterile medium containing agar (20 g/L) onto Corning (Corning, NY) 100 × 20 mm polystyrene plates. Liquid cultures were incubated at 30 °C on a rotary shaker, and solid cultures were maintained at 30 °C in an incubator.

Sample preparation. 750-ml overnight cultures of *S. cerevisiae* were grown to stationary phase (OD_{600} of ~1.7 as measured with a Shimadzu PharmaSpec UV-1700 UV-vis spectrophotometer). This culture was divided equally into 50-ml Falcon centrifuge tubes.

Stock solutions of AmdeB, AmB and Erg were prepared in DMSO. MBCD was added directly to the liquid culture. Cells were treated with either a DMSO-only control, 5 µM AmdeB or 5 µM AmB for 1 min, 30 min, 60 min or 120 min. Cells were treated with DMSO control, 500 mM MBCD, 25 µM Erg control and the 5 µM AmB/25 µM Erg complex (section VII) for 120 min. Treated tubes were incubated on the rotary shaker (200 r.p.m.) at 30 °C for the time of exposure.

To quantify colony-forming units (CFUs), at the end of exposure, aliquots were taken from the samples, diluted and plated on YPD agar plates. The plates were then incubated for 48 h at 30 °C, and colony-forming units were counted.

To quantify the percentage of Erg remaining, yeast membranes were isolated using a modified version of Haas' spheroplasting and isosmotic cell lysis protocol and simple differential ultracentrifugation[45]. At the end of the exposure time, tubes were removed from the shaker and centrifuged for 5 min at 3,000*g* at room temperature. The supernatant was decanted, and 5 ml of wash buffer (dH_2O, 1 M DTT, 1 M Tris-HCl, pH 9.4) was added. The tubes were vortexed to resuspend and incubated in a 30 °C water bath for 10 min. Tubes were then centrifuged again for 5 min at 3,000*g*, and the supernatant was decanted.

1 ml of spheroplasting buffer (1M KPi, YPD medium, 4 M Sorbitol) and 100 µl of a 5 mg/ml solution of lyticase from *Arthrobacter luteus* (L2524 Sigma-Aldrich) was added to each tube, and each tube was then vortexed to resuspend. Tubes were incubated in a 30 °C water bath for 30 min, with occasional swirling. After incubation, tubes were centrifuged for 10 min at 1,080*g* at 4 °C, and the supernatant was decanted.

1 ml of PBS buffer and 20 µl of a 0.4 mg/ml dextran in 8% Ficoll solution was added to each tube and mixed very gently to resuspend. This suspension was placed on ice for 4 min and then heat shocked in a 30 °C water bath for 3 min.

The suspensions were then transferred to Eppendorf tubes, vortexed to ensure complete lysis, and centrifuged at 15,000*g* at 4 °C for 15 min to remove unlysed cells and cell debris. The resulting supernatants were transferred to thick-wall polycarbonate ultracentrifuge tubes (3.5 ml, 13 × 51 mm, 349622 Beckman Coulter) and spun for 1 h at 100,000*g* at 4 °C in a Beckman Coulter TLA-100.3 fixed-angle rotor in a Beckman TL-100 ultracentrifuge. The supernatant was poured off. The remaining membrane pellet was resuspended in 1 ml PBS buffer and stored at −80 °C until further analysis.

Gas chromatography quantification of sterols. 750 µl of each membrane pellet sample and 20 µl of internal standard (4 mg/ml cholesterol in chloroform) were dissolved in 3 ml 2.5% ethanolic KOH in a 7-ml vial, which was then vortexed gently, capped and heated in a heat block on a hot plate at 90 °C for 1 h. The vials were then removed from the heat source and allowed to cool to room temperature. 1 ml of brine was added to the contents of each vial. Extraction was performed twice, each with 3 ml of hexane. Organic layers were removed in both extractions, dried over magnesium sulfate, filtered through Celite 545 (Sigma-Aldrich) and transferred to another 7 ml vial. The contents of the vial were then concentrated *in vacuo* in a 30 °C water bath.

The resulting sterol films were resuspended in 100 µl pyridine and 100 µl *N*,*O*-bis-(trimethylsilyl)-trifluoroacetamide with 1% trimethylchlorosilane (T6381-10AMP Sigma-Aldrich) by vortexing gently[57]. This solution was heated at 60 °C for 1 h. The vials were placed on ice, and the solvent was evaporated off by nitrogen stream. Vials must be kept at a low temperature to prevent evaporation of the sterol TMS ethers along with the solvent. The resulting films were resuspended in 100 µl of decane, filtered and transferred to a GC vial insert for analysis.

Gas chromatography analysis was carried out on an Agilent 7890A gas chromatograph equipped with a FID, an Agilent GC 7693 Autosampler and a Dell computer running Microsoft XP that uses ChemStation v.B.04.02 SP1. Samples were separated on a 30-m, 0.320-mm ID, 0.25-µm film HP-5 capillary column (19091J-413 Agilent) using hydrogen as a carrier gas with an average velocity of 84.8 cm/s. Nitrogen make-up gas, hydrogen and compressed air were used for the FID. A split/splitless injector was used in a 20:1 split. The injector volume was 2 µl. The column temperature was initially held at 250 °C for 0.5 min and then was ramped to 265 °C at a rate of 10 °C/min, with a final hold time of 12.5 min. The injector and detector temperature were maintained at 270 °C and 290 °C, respectively. The value reported for each time point was calculated by dividing the value for the treatment group by the value for the DMSO control at the same time point and then normalizing the DMSO control to 100%.

V. Preparation of an amphotericin–Erg complex. Erg was prepared as a stock solution (4 mg/ml in $CHCl_3$), and the solvent was removed under a gentle stream of nitrogen gas. Residual solvent was removed under high vacuum for at least 8 h. A DMSO solution of 5 µM AmB was then added to this solid Erg (25 µM final Erg concentration; 5:1 mol ratio Erg/AmB). The resulting suspension was gently vortexed and then heated to 80 °C for 1 h in an aluminum heating block to allow Erg to fully dissolve. The resulting AmB-Erg solution was then allowed to cool to room temperature. This solution was left to complex at room temperature for another hour before use.

The absorbance spectra of the two types of aggregate, (i) 5 µM AmB only in PBS buffer and (ii) 5 µM AmB/25 µM Erg complex in PBS buffer, as well as the monomeric form of AmB (AmB in 25% PBS buffer, 75% methanol) were investigated using a Shimadzu PharmaSpec UV-1700 UV-vis spectrophotometer[58]. **Supplementary Figure 15** shows the distinct shift in UV spectra between the different forms of AmB and AmB bound to Erg in a complex.

51. Seo, S. *et al.* Biosynthesis of sitosterol, cycloartenol, and 24-methylenecycloartanol in tissue-cultures of higher-plants and of ergosterol in yeast from [1,2-$^{13}C_2$]- acetate and [2-^{13}C-$^{2}H_3$]-acetate and [5-$^{13}C_2$-$^{2}H_2$] MVA. *J. Chem. Soc. Perkin Trans. I* 2407–2414 (1988).
52. Pangborn, A.B. *et al.* Safe and convenient procedure for solvent purification. *Organometallics* **15**, 1518–1520 (1996).

doi:10.1038/nchembio.1496

53. Comellas, G., Lopez, J.J., Nieuwkoop, A.J., Lemkau, L.R. & Rienstra, C.M. Straightforward, effective calibration of SPINAL-64 decoupling results in the enhancement of sensitivity and resolution of biomolecular solid-state NMR. *J. Magn. Reson.* **209**, 131–135 (2011).
54. Morcombe, C.R. & Zilm, K.W. Chemical shift referencing in MAS solid state NMR. *J. Magn. Reson.* **162**, 479–486 (2003).
55. Rienstra, C.M. *et al.* Determination of multiple torsion-angle constraints in U-^{13}C,^{15}N-labeled peptides: 3D ^{1}H-^{15}N-^{13}C-^{1}H dipolar chemical shift NMR spectroscopy in rotating solids. *J. Am. Chem. Soc.* **124**, 11908–11922 (2002).
56. Ohi, M., Li, Y., Cheng, Y. & Walz, T. Negative staining and image classification—powerful tools in modern electron microscopy. *Biol. Proced. Online* **6**, 23–34 (2004).
57. Winkler, J.K., Rennick, K.A., Eller, F.J. & Vaughn, S.F. Phytosterol and tocopherol components in extracts of corn distiller's dried grain. *J. Agric. Food Chem.* **55**, 6482–6486 (2007).
58. Shervani, Z. *et al.* Aggregation of polyene antibiotics as studied by electronic absorption and circular dichroism spectroscopies. *Colloid. Surface. B* **7**, 31–38 (1996).